Draft version October 5, 2016
Preprint typeset using LaTeX style emulateapj v. 08/22/09

arXiv:1610.00801v1 [astro-ph.GA] 4 Oct 2016

THE QUEST FOR THE LARGEST DEPLETED GALAXY CORE: SUPERMASSIVE BLACK HOLE BINARIES AND STALLED IN-FALLING SATELLITES

Paolo Bonfini*
Centre for Astrophysics and Supercomputing, Swinburne University of Technology, Victoria 3122, Australia.
Current address: Centro de Radioastronomía y Astrofísica, UNAM, Campus Morelia, México.

Alister W. Graham
Centre for Astrophysics and Supercomputing, Swinburne University of Technology, Victoria 3122, Australia.
Draft version October 5, 2016

Abstract

Partially-depleted cores are practically ubiquitous in luminous early-type galaxies ($M_B \lesssim -20.5$ mag), and typically smaller than 1 kpc. In one popular scenario, supermassive black hole binaries — established during dry (i.e. gas-poor) galaxy mergers — kick out the stars from a galaxy's central region via three-body interactions. Here, this "binary black hole scouring scenario" is probed at its extremes by investigating the two galaxies reported to have the largest partially-depleted cores found to date: 2MASX J09194427+5622012 and 2MASX J17222717+3207571 (the brightest galaxy in Abell 2261). We have fit these galaxy's two-dimensional light distribution using the core-Sérsic model, and found that the former galaxy has a core-Sérsic break radius $R_{b,cS} = 0.55$ kpc, three times smaller than the published value. We use this galaxy to caution that other reportedly large break radii may too have been over-estimated if they were derived using the "sharp-transition" (inner core)-to-(outer Sérsic) model. In the case of 2MASX J17222717+3207571, we obtain $R_{b,cS} = 3.6$ kpc. While we confirm that this is the biggest known partially-depleted core of any galaxy, we stress that it is larger than expected from the evolution of supermassive black hole binaries — unless one invokes substantial gravitational-wave-induced (black hole)-recoil events. Given the presence of multiple nuclei located (in projection) within the core radius of this galaxy, we explored and found support for the alternative "stalled infalling perturber" core-formation scenario, in which this galaxy's core could have been excavated by the action of an infalling massive perturber.

Subject headings: keyword: galaxies: elliptical and lenticular, cD — galaxies: individual (2MASX J17222717+3207571, 2MASX J09194427+5622012) — galaxies: photometry — galaxies: structure

1. INTRODUCTION

The spheroidal component of many luminous early-type galaxies (ETGs; $M_B \lesssim -20.5 \pm 0.75$ mag) are characterized by the presence of a depleted stellar core, which manifests itself as a marked flattening of the inner light distribution relative to the inward extrapolation of the spheroid's outer Sérsic profile (e.g. Graham et al. 2003). Galaxies with shallow inner surface brightness profiles have of course been observed for decades (e.g. King & Minkowski 1966, 1972) but it has not always been reliably established if this represents a deficit of stars relative to the outer profile, nor have the sizes of these cores been robustly measured. It is important to realize that a flat core does not necessarily represent a signature of a depleted core, and flat cores can even arise from the presence of additional nuclear components (see Dullo & Graham 2012, 2013, their Appendix A.2). Furthermore, several brightest cluster galaxies (BCGs; e.g. Donzelli et al. 2011), and even some cD galaxies embedded in halos of intracluster light (NGC 4874 and UGC 9799; Seigar et al. 2007), are characterized by low Sérsic index spheroids whose flat inner light profiles do not deviate from their outer Sérsic profile.

In Bonfini et al. (2015) we demonstrated that the galaxy Holm 15A, alleged to have the largest depleted core on record (4.6 kpc López-Cruz et al. 2014), actually has no central deficit relative to its outer Sérsic profile which also describes the inner profile. This is important because the original investigation led to *(a)* the claim of a massive depleted core and in turn *(b)* the possible presence of a truly massive 10^{11} $M_\odot$ black hole. Remarkably, our results were later independently confirmed by the study of Madrid & Donzelli (2016), who also described Holm 15A as "core-less".

The same situation may well have occurred with the analysis of a similar-looking light profile, from the central galaxy in the MS0735.6+7421 cluster, for which McNamara et al. (2009) report a depleted core with a radius of 3.8 kpc — which they wrote supported the evidence for an ultramassive black hole. Compounding matters, the allegedly largest black hole mass directly measured via dynamical methods, specifically $M_\bullet = 1.7 \pm 0.3 \times 10^{10}$ $M_\odot$ in NGC 1277 (van den Bosch et al. 2012), was later reduced to 5×10^9 $M_\odot$ (Emsellem 2013; Walsh et al. 2015) and is likely less than 1.2×10^9 $M_\odot$ (Graham et al. 2016). Furthermore, it appears that the masses of most AGNs may have been over-estimated by a factor of a few, due to an incorrectly calibrated virial factor (Shankar et al. 2016). Collectively, this casts some doubt on the abundance of ultramassive black holes, and,

Electronic address: *p.bonfini@crya.unam.mx

more specifically, reveals the need for an independent confirmation of large black hole masses and large partially depleted cores. Here we investigate the next two largest cores reported in the literature.

One of the favored scenarios for the formation of depleted stellar cores involves binary supermassive black holes (SMBHs; Begelman et al. 1980; Ebisuzaki et al. 1991; Quinlan 1996; Yu 2002; Merritt & Milosavljević 2005). It has been suggested that SMBH binaries, established during dry (i.e. gas-poor) mergers which built the ETG, remove stars on radial orbits crossing the galaxy nucleus via three-body interactions. This activity is performed at the expense of the potential energy of the binary, which ultimately coalesces into a central SMBH. Observational evidence supporting this theory is provided by the existing scaling relations between the mass of the SMBH and the characteristic radius of the depleted core, or the depleted stellar mass (e.g. Graham 2004; Ferrarese et al. 2006; Lauer et al. 2007). However, predictions from the SMBH binary scenario cannot readily account for the extremely large cores, and hence depleted masses, reported for several ETGs (i.e. core radius > 1 kpc; e.g. Laine et al. 2003; Lauer et al. 2007; Postman et al. 2012; Hyde et al. 2008), unless it is assumed that the host galaxy underwent extraordinary merging activity (see the discussion in Bonfini et al. 2015). Reports of such large cores is therefore casting shadows on the SMBH scouring scenario as the sole mechanism for core formation.

Several alternative models for the formation of cores can not yet boast the same observational support which the SMBH scouring scenario received over the last few decades, but they are gaining attention due to their ability to reproduce larger cores (which may or may not be real). Among these alternatives, the most noticeable is (arguably) the "ejected SMBH" scenario (e.g. Redmount & Rees 1989; Merritt et al. 2004; Boylan-Kolchin et al. 2004; Gualandris & Merritt 2008). According to this framework, the coalescence of the SMBH binary causes the newly formed SMBH to recoil following the anisotropic emission of gravitational waves in the other direction (Bekenstein 1973; Fitchett & Detweiler 1984; González et al. 2007). Potentially, the SMBH may be expelled from the galaxy core, or placed on a radial orbit recurrently intersecting with the nucleus. This phenomenon is able to significantly enlarge the core produced during the SMBH binary phase (up to $\sim$5% of the galaxy half-light radius; Gualandris & Merritt 2008). Arguments against this model have been raised in regard to the "final parsec problem", i.e. the possible stalling of the SMBH binary separation (preventing the final coalescence) due to the depletion of core stars capable of transferring momentum (Milosavljević & Merritt 2003). However, recent works based on realistic galaxy potentials considering triaxiality, asymmetry, eccentricity of the SMBHs orbits, or rotation have shown that the binary evolution is convergent (e.g. Khan et al. 2013; Merritt 2015; Holley-Bockelmann & Khan 2015; Vasiliev et al. 2015). The SMBH recoil scenario has been recently advocated by Markakis et al. (2015) to explain the $\sim$0.2 kpc core they observed in the peculiar galaxy NGC 3718.

Another promising model for the explanation of large cores is the "stalled perturber" scenario. In a seminal paper, Chandrasekhar (1943) suggested that the dynamical friction exerted by a homogeneous mass distribution can cause a captured object to spirally infall due to the transfer of angular momentum from the infalling object to the background particles (stars), which are moved to larger orbits. More recently, Read et al. (2006a) reviewed the assumption of homogeneous mass distribution, and demonstrated instead that a necessary condition for the spiral infall is that the background particles cannot have a constant density distribution. In particular, numerical simulations have shown that the infall of a clumpy baryonic perturber makes a central "cuspy" dark matter distribution shallower, and can even convert it to a constant density core (e.g. El-Zant et al. 2001; Merritt & Milosavljević 2002; El-Zant et al. 2004; Merritt et al. 2004; Tonini et al. 2006). Goerdt et al. (2010) suggests that a baryonic/stellar core forms because the cusp is literally shredded by the tidal interaction with the perturber (see also Petts et al. 2015).

Apart from the "ejected SMBH" and the "stalled infalling perturber" models considered above, other models allow for extremely large cores/mass deficits, such as the "multiple-SMBH scouring" scenario of Kulkarni & Loeb (2012), or the combined "sinking SMBH – AGN feedback" scenario of Martizzi et al. (2012). However, the predictions from those models require much more tuning, and they are somewhat difficult to explore observationally.

It is important to confirm claims of unusually large cores in order to: *a*) check on the need for scenarios proposed to explain them, and *b*) constrain the existing scaling relations between the characteristics of the core and the mass of the black hole ($M_\bullet$; e.g. Rusli et al. 2013; Dullo & Graham 2014). Massive ETGs are expected to host the most massive SMBHs and have the widest cores. Although larger cores should be the easiest to measure, our recent study of Holm 15A revealed that misinterpretations are still possible. These considerations motivated us to revisit the large cores reported in two galaxies: 2MASX J17222717+3207571, the BCG of Abell 2261 (hereafter A2261-BCG; $R_{core} = 3.2$ kpc; Postman et al. 2012), and 2MASX J09194427+5622012 (or SDSS-J091944.2+562201.1, hereafter SDSS-H5;[1] $R_{core} = 1.6$ kpc; Hyde et al. 2008). Details on these galaxies are reported in Table 1.

As warned in Graham et al. (2003), the Nuker model (Lauer et al. 1995) can incorrectly imply the presence of a partially depleted core when there is an undisturbed (non-depleted) Sérsic profile with a low Sérsic index. This occurred in — for example — NGC 4473 (Pinkney et al. 2003; see Dullo & Graham 2014) and Holm 15A (López-Cruz et al. 2014; see Bonfini et al. 2015). As was also explained in Graham et al. (2003), the Nuker model "break radius" can significantly overestimate the sizes of cores (see Trujillo et al. 2004 and Dullo & Graham 2012, 2014) which led to the alternative use of the radius where the negative logarithmic slope of the radial intensity profile equals 0.5. However every light profile has such a radius, irrespective of whether or not it actually contains a partially depleted core. It is therefore necessary to test if there is an in-

[1] Our naming simply follows the indexing of the sample in Hyde et al. (2008).

TABLE 1
SAMPLE

Target	z	D_L [Mpc]	$m-M$ [mag]	Scale [kpc/″]	Camera/Filter	Exposure [sec]	Pixel Scale [″/pixel]
(1)	(2)	(3)	(4)	(5)	(6)	(7)	(8)
2MASX J17222717+3207571 (A2261-BCG)	0.225	1119	40.24	3.61	ACS/F814W	4099	0.050
2MASX J09194427+5622012 (SDSS-H5)	0.278	1423	40.77	4.22	HRC/F775W	1200	0.025

NOTE. — Basic information for the sample galaxies, and for the HST images used in the current work. (1) Target name. (2) Redshift measurement from SDSS-DR1 (Abazajian et al. 2003) for SDSS-H5, and from NED (Virgo + GA + Shapley) for A2261-BCG. (3) Luminosity distance, assuming a cosmology with $H_0 = 70$ km s^{-1} Mpc^{-1}, $\Omega_\Lambda = 0.7$, and $\Omega_m = 0.3$. (4) Distance modulus. (5) Scale at the luminosity distance of column 3. (6) HST camera and filter. (7) Total exposure time. (8) Instrument pixel scale.

ner deficit of light relative to the outer light profile. In this work we use the core-Sérsic model to do this. While A2261-BCG has so far only been fit with a Nuker model, SDSS-H5 has already been fit with a core-Sérsic model by Hyde et al. (2008). However, we identified some concerns with their approach (see §5) and we therefore perform an independent fit analysis, finding a core which is three times smaller for the reasons explained within.

This paper is structured as follows. In §2, we present the data. In §3 we outline our strategy for the 2D fit of the surface brightness distribution, while in §4 we present the results of this analysis. In §5 we discuss our results in the context of different formation scenarios for (massive) depleted cores. Finally, we summarize our conclusions in §6. Throughout the paper, we assume a cosmology with $H_0 = 70$ km s^{-1} Mpc^{-1}, $\Omega_\Lambda = 0.7$, and $\Omega_m = 0.3$.

2. DATA

Our analysis is performed on archival *HST* images obtained in the *I*-band. This provided the best compromise between high spatial resolution and minimal dust contamination[2], both desirable in the study of galaxy cores. In particular, we retrieved deep ACS/F814W (Johnson-Cousins *I*) and ACS-HRC/F775W (SDSS *i*) images for A2261-BCG and SDSS-H5, respectively, from the STScI MAST Archive (see Table 1 for image specifics). The same camera/filter sets were also used by Postman et al. (2012) and Hyde et al. (2008), therefore allowing for a direct comparison. For each galaxy, we combined the different exposures using the AstroDrizzle tool (v1.1.16; Fruchter et al. 2010) through the PyRAF (v2.1.6) suite[3], sampling the images at the native pixel scale of each camera (see Table 1), which was more than sufficient to study the cores of our sample galaxies.

2.1. *Masking*

We masked the contaminating objects in the field using the detections obtained from a double run of SExtractor (Bertin & Arnouts 1996), tuned first to identify point-like sources and then extended objects. We then additionally masked cosmic rays, chip imperfections, and internal reflections after visual inspection. The masked areas are shown in the images of Figure 1 (top-panels) as darkened regions.

Notice that we did not mask a bright object S–E of the center of A2261-BCG; given the significant overlap/contamination, we preferred instead to model it concurrently with A2261-BCG. Similarly, we did not mask the bright "knots" around the core of this galaxy (Figure 1, inset of the top-left panel) but instead modelled them. In their analysis, Postman et al. (2012) labelled these knots with progressive numbers from 1 to 4 (in clockwise order in the image), a nomenclature which we retain here for the sake of comparison. However, from our initial 2D fit residuals, we identified a fifth knot ("knot 5"), not directly visible in this image. Knots 1—5 have been included as additional components in our fit, similarly to the bright object S–E of the center. The nature of these knots will be discussed in §5.

2.2. *PSF and sigma image*

Our 2D fitting algorithm Galfit-Corsair (Bonfini 2014; see also §3) convolves, at each iteration, the model with the point spread function (PSF), and then compares the result against the data. To create realistic PSFs for our images, we first used the TinyTim tool (Krist et al. 2011) to produce "distorted" *HST* PSFs, i.e. as they would appear in the native *HST* fields (without applying the HST distortion geometry corrections). We then run these PSF images through AstroDrizzle using the exact same setup used to create the mosaics. In this way we obtained artificial PSFs whose features (e.g. diffraction spikes) are oriented exactly as those of the point-like sources in the mosaics. Moreover, this process allowed us to to mimic the "pixellation" imprint which AstroDrizzle produced on the mosaicked images.

AstroDrizzle can provide variance maps as an additional output of the mosaicing process. Apart from the Poissonian errors on the source and background fluxes, these variance images include the flat-fielding uncertainties and the correlated pixel noise. However, since in the mosaics of both galaxies the galaxy light contaminates the sky background (see §3.1), which is by far the main responsible for the "error budget", we preferred not trust the internal AstroDrizzle algorithm for the sky estimation, and decided to generate our own weight

[2] We performed a visual inspection of the F225W (WFC3/UVIS), F475W (ACS), and F606W (ACS) images for A2261-BCG, and of the F475W (ACS) image for SDSS-H5, and found no obvious trace of dust contamination, although it is not excluded that — given the large distance of the galaxies — unresolved dust lanes might still be present.

[3] PyRAF is a product of the Space Telescope Science Institute, which is operated by AURA for NASA.

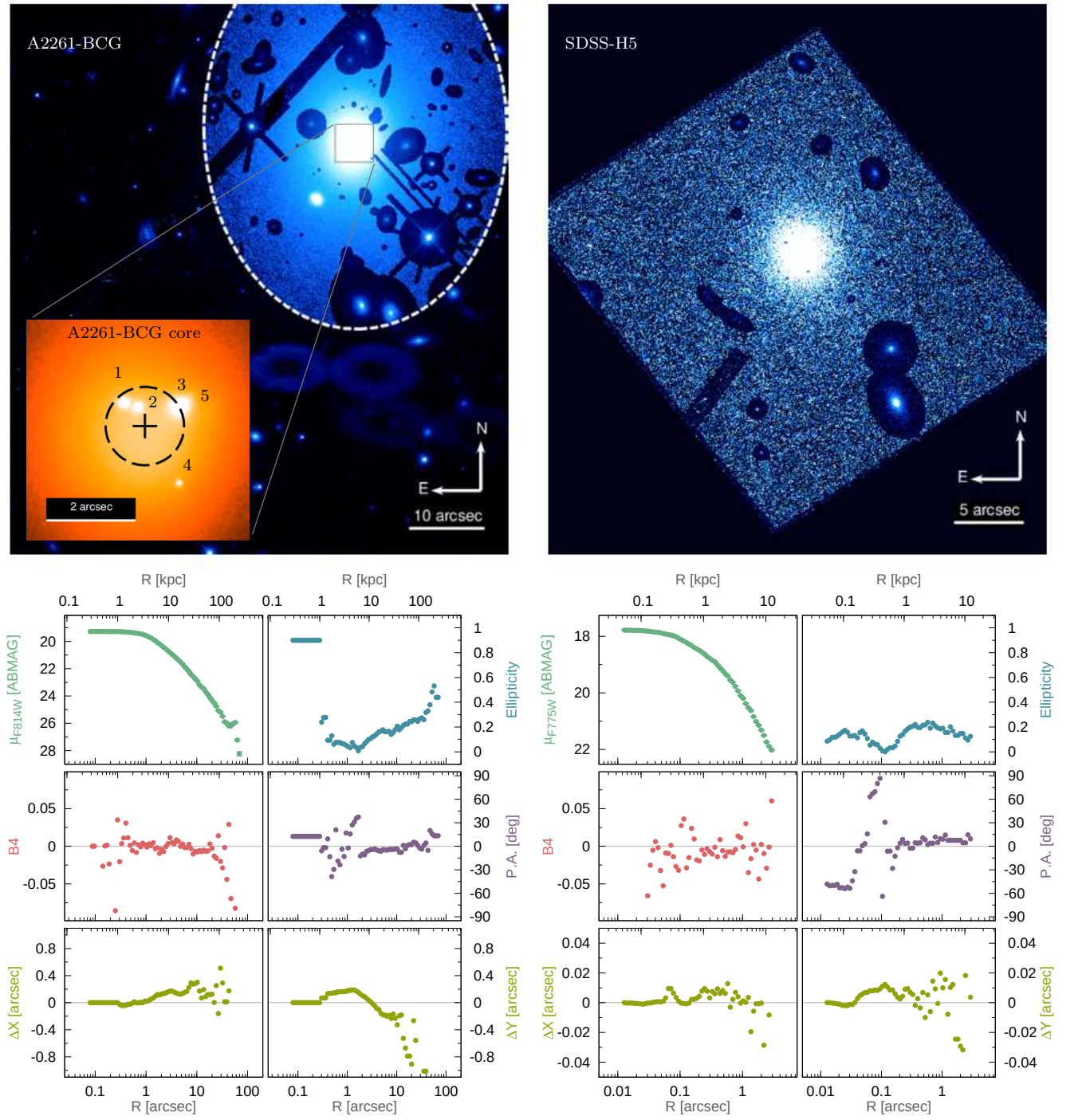

FIG. 1.— *HST* images of the sample galaxies, and preliminary 1D analysis for A2261-BCG (*left*) and SDSS-H5 (*right*). *Top.*- *HST* mosaics produced with the procedure described in §2. The darker regions correspond the areas excluded (masked) from our analysis (see §2.1). The dashed white ellipse in the top-left panel corresponds to the physical extent of our 2D fit (see §3). The insert in the top-left panel is a zoom into the central regions of A2261-BCG. The dashed black circle represents the size of the core as measured by Postman et al. (2012), and its center (black cross) corresponds to the centroid of the innermost elliptical isophote found with our IRAF.*ellipse* analysis (see §3.1). The objects (1 – 4) around the core have been labelled following Postman et al. (2012). After subtracting the modelled galaxy light, we revealed an additional object (5), not visible in this representation. *Bottom.*- IRAF.*ellipse* major-axis radial profiles for: surface brightness (*top-left*), ellipticity (*top-right*), *4th* harmonic deviation from perfect ellipticity (*B4*; *middle-left*), position angle (*middle-right*), and isophote centroid shift along the *x*-axis (*bottom-left*) and *y*-axis (*bottom-right*) with respect to the innermost isophote. The photometric errors of the surface bright ness data points are typically within the size of the data symbols.

images. The weight (or "sigma") image for SDSS-H5 was created using the GALFIT-CORSAIR algorithm (inherited from GALFIT), which uses a sigma-clipping technique to derive the image noise characteristics. Instead, for the sigma image of A2261-BCG — whose field is significantly crowded — we preferred to proceed following the procedure described in Bonfini (2014, their Section 3.2.1). In brief, we performed the sum in quadrature of the Poissonian noise of the source counts plus the background noise. The background noise is in turn the sum in quadrature of the noise due to the readout, the detector dark current, and the sky. While the first two are known (since they are characteristics of the camera), the latter had to be estimated. The WFC3 Instrument Handbook (Dressel 2015, their Table 9.7.1) provides rough estimates for the surface brightness of the zodiacal light (the dominant component of sky background in typical observing conditions) in the V-band, as a function of elliptical coordinates. We used the astrometric information in our images to pick the relevant V-band sky magnitude from these values, and converted them to I-band (as we were using the F814W and F775W filters) using an average sky color $V - I \sim 0.6$ mag (e.g. Vaccari 2000). This provided us with an independent estimate for the sky magnitudes, which were converted into counts using the exposure information. Finally, the sky noise was calculated applying Poissonian statistics over these expected sky counts.

3. MODELLING

We performed two-dimensional fits to the surface brightness distribution of the galaxies using GALFIT-CORSAIR[4] (Bonfini 2014), an advancement of the GALFIT software (Peng et al. 2010) which we developed to include the core-Sérsic model (Graham et al. 2003). The 2D approach has the advantage of being able to simultaneously fit (rather than mask) contaminant objects. This ability is particularly handy for the case of A2261-BCG, since several objects lie (along the line of sight) within its central regions (see Figure 1, top-left panel), and they could affect the estimate of, and be related to, the core size. In our recent work (Bonfini 2014; Bonfini et al. 2015), we showed that 2D fitting proved to agree with 1D analysis modulo strong radial ellipticity gradients (which are of minor concern in the present case; see the ellipticity profiles in Figure 1, and §3.1 for how they were measured).

3.1. *Preliminary photometry*

When creating the mosaics, we used the default ASTRODRIZZLE setup except for the automatic sigma-clipping sky subtraction, due to the relatively large extent on the chip of the galaxy (in the case of SDSS-H5) and for the high source density around A2261-BCG. Instead, we evaluated the sky-background by hand, measuring it at the edges of the images over several "boxes" located at different azimuthal angles around each galaxy, and then adopting the median value, which was then subtracted from the images. The boxes were located at galactocentric distances of $\sim$10 R_e and $\sim$4 R_e, for A2261-BCG and SDSS-H5 respectively. Therefore, especially for the case of SDSS-H5, we could not exclude that our assumed background was contaminated by the galaxian light. The influence of this uncertainty on our best-fit parameters has been quantified via the Monte Carlo simulation presented in the Appendix.

The "first-guess" parameters for the models have been chosen after inspecting the various 1D profiles, measured along elliptical isophotes using the IRAF.*ellipse* task (Jedrzejewski 1987). While the IRAF.*isofit* task (Ciambur 2015) is superior, it produces similar results when dealing with rather round ETGs that do not contain edge-on disks. The bottom panels of Figure 1 show the surface brightness (μ) of the galaxies, extracted along the semi-major axis, along with the radial profiles of: ellipticity (e); $4th$ harmonic deviation from perfect ellipticity ($B4$ "boxiness/diskiness" parameter); position angle (P.A.); and isophote centroid shift.

In running IRAF.*ellipse* on the image of A2261-BCG, we excluded the knots 1–5 and the overlapping companion galaxy, which were included in our 2D fit (see §2.1 and Figure 3). Due to the large fraction of masked pixels and the relatively mild slope of the brightness profile in the core region, the centering algorithm of IRAF.*ellipse* failed within the innermost $\sim$3″of A2261-BCG. The data points within this limit are therefore measured along concentric ellipses of identical ellipticity, P.A., and center. However, as already noticed in Postman et al. (2012, their Figure 4), a contour plot of the galaxy reveals that, within the core, the center of the isophotes are slightly shifted N–W by $\sim$1″ with respect to the outer isophotes (see §3.2). This feature will be addressed further in §5.

3.2. *Fitting*

We fit the surface brightness distribution of the galaxies using a 2D core-Sérsic model (Graham et al. 2003), which provides a smooth connection between an outer Sérsic component and an inner power-law component. The core-Sérsic profile can be expressed as:

$$I(R) = I' \left[1 + \left(\frac{R_{b,cS}}{R}\right)^{\alpha}\right]^{\gamma/\alpha} \exp\left[-b_n \left(\frac{R^{\alpha} + R_b^{\alpha}}{R_e^{\alpha}}\right)^{1/(n\alpha)}\right] \quad (1)$$

with

$$I' = I_b 2^{-\gamma/\alpha} \exp\left[b_n 2^{1/n\alpha} (R_{b,cS}/R_e)^{1/n}\right] \quad (2)$$

where $R_{b,cS}$ (core-Sérsic "break radius") is the radius corresponding to the mid-point between the outer Sérsic and the inner power-law portion of the profile. The parameter α modulates the sharpness of the changeover, and I_b represents the intensity at $R_{b,cS}$. The asymptotic inner power law slope is given by γ, while the outer Sérsic index is identified by n. Finally, b_n is a normalization factor which can be defined to make R_e the effective half-light radius of the non-depleted Sérsic profile (see Graham et al. 2003). We remark that use of α, when the transition between the core and outer region is broad, is important for not over-estimating the size of the break radius.

In this context, the break radius $R_{b,cS}$ is adopted as a parametric measurement of the core size. This is a formally defined point, and it should borne in mind that a

[4] www.astronomy.swin.edu.au/~pbonfini/galfit-corsair/

SMBH binary which excavates a core can affect a galaxy light profile up to radii well beyond the break radius. In fact, stars on extremely elongated (almost radial) orbits can intersect with the sphere of influence of the SMBH binary, and hence be ejected. It is of course possible to designate alternative "core sizes" defined relatively to the deviation from the outer Sérsic fit. However, any radius corresponding to a the deviation from the outer Sérsic fit of, say, 0.1%, or 0.5%, or x%, will occur far out in the profile for finite values of alpha (since the core-Sérsic and its Sérsic part only converge for $R \rightarrow \infty$). Moreover, any such radius is arbitrary and therefore not a radius that is important. Notice that the physical quantity of actual interest in the study of depleted cores — the "luminosity (or mass) deficit" — is independent, in our analysis, from the definition of $R_{b,cS}$, being the difference between the integrated luminosity (or mass) of the extrapolated Sérsic profile and that of the actual core-Sérsic profile.

The fit area was extended to the whole image in the case of SDSS-H5, while it was arbitrarily limited within the isophote with a semi-major axis of $27''.5$ (corresponding to a surface brightness of 25.5 mag arcsec^{-2} in the F814W filter) for A2261-BCG. The fit areas appear as brighter regions in the top panels of Figure 1.

For the knots within the core region of A2261-BCG, we initially assumed point-like models (i.e. PSFs), and then iteratively increased the complexity of the components after inspection of the residuals (first using Gaussian and then Sérsic models). In our final fit, knots 1–3 are described by Sérsic components, while knots 4 and 5 by point-like sources. The companion galaxy S–E of A2261-BCG was fit with a Sersic model.

Given the isophote centroid shift within the core region of A2261-BCG (see Figure 1), we decided to perform an additional fit limited to $5''$ in order to allow a local recentering of the underlying core-Sérsic component. This analysis obtained a better fit of the knots, rather than a refined estimate of the core size (for which the measurement of the outer Sérsic profile is fundamental; see §5.1).

4. RESULTS

Our measured core-Sérsic parameters for the galaxies are reported in Table 2, while the results from the modelling of the knots of A2261-BCG are presented in Table 3. In the same tables, we also report the stellar masses of each galaxy's spheroid ($M_{\rm sph,*}$) derived from the integrated stellar luminosities assuming the stellar mass-to-light (M/L) ratio given in Table 2. This M/L was estimated using the "Worthey model interpolation engine" applet[5] based on the evolutionary models by Worthey (1994), where we adopted the default (Salpeter) initial mass function prescriptions, assuming a uniformly old (12 Gyrs), solar metallicity stellar population (as typical for massive early-type galaxies, e.g. Gallazzi et al. 2006). The errors on the best-fit parameters reported in Table 2, which represent 50% confidence levels, are mostly due to the uncertainty on the background level (which largely dominates over the Poissonian uncertainty obtained by reversing the best-fit covariance matrix). These errors were estimated by simulating different sky levels for the images, and then repeating the same fits in order to evaluate the possible range for each parameter. The details of the estimation of the parameter errors are given in the Appendix.

In Figure 2 we present the fit residuals (image − model) obtained with GALFIT-CORSAIR for A2261-BCG (left) and SDSS-H5 (right). The insert in the left panel shows the residuals for the fit of the $5''$ core region of A2261-BCG.

The top panels of Figure 3 present the 1D projections of the surface brightness of the models (blue solid curve) measured along the same galaxy isophotes identified with our IRAF.*ellipse* analysis of each image (see §3.1). It should be noted that these 1D projections are not the fit, which was performed in 2D, but simply show the match along this single profile. We also show the projections of the individual components of each model with grey lines, and we compare these projections against the actual surface brightness of the galaxies (green data points). As a term of comparison we also show, with a dashed purple line, the extrapolation of the Sérsic part of the core-Sérsic component. The projections of the 1D residuals (plotted in the lower panels underneath the surface brightness profiles) are presented both in terms of the surface brightness difference ($\Delta\mu$), and in terms of standard deviations. Notice that the 1D projections are centered on the galaxy center, therefore the additional objects that we fit concurrently with A2261-BCG appear offset in this 1D representation. For SDSS-H5, despite the fit being extended to practically the whole image (top-right panel of Figure 1), the 1D projection is limited by the largest isophote identified by IRAF.*ellipse*.

We observed that, by limiting the spatial extent of the fit of A2261-BCG to the central region, the center of the core-Sérsic component shifted noticeably, as expected from the previously identified centroid shift (see §3.1). The shift of the centroid of our 2D model is obviously a function of the fit extent; by experimenting with increasingly smaller spatial limits, we found a shift of $\sim 0''.05$ – $0''.10$, corresponding to a physical distance of a few hundreds parsecs.

From the core-Sérsic fit to A2261-BCG we obtained a large break radius $R_{b,cS} = 3.63$ kpc, while for SDSS-H5 we obtained a more "modest" $R_{b,cS} = 0.55$ kpc. In §5.1 we compare these core sizes with the results obtained in the studies of Postman et al. (2012, A2261-BCG) and Hyde et al. (2008, SDSS-H5), and we relate them to the typical values observed in early-type galaxies.

4.1. *Mass deficits*

The mass deficit (M_{def}; i.e. the stellar mass removed to create the core), can be calculated from the luminosity deficit (L_{def}), which is defined as the difference between the assumed pre-depletion light profile and the one actually observed. In the core-Sérsic framework, L_{def} can be calculated as the difference between the whole core-Sérsic model (the observed light profile), and the inward extrapolation of its Sérsic part (the presumed pristine light profile). In these regards, we remark that our measurement of the central mass deficit is relative to the extrapolation of the outer profile. That is, we measure the difference between the mass derived from the actual light distribution, and what this mass would be if the spheroid's outer Sérsic profile continued into the galaxy

[5] http://astro.wsu.edu/worthey/dial/dial_a_model.html

TABLE 2
Best-fit core-Sérsic Parameters

Target	Filter	$\mu^{\dagger}_{b,filter}$ [mag/$''^2$]	$m^{\dagger}_{filter}$ [mag]	$R_{b,cS}$ [$''$] / [kpc]	α	γ	R_e [$''$] / [kpc]	n	e	$P.A.$ [deg]
(1)	(2)	(3)	(4)	(5)	(6)	(7)	(8)	(9)	(10)	(11)
A2261-BCG	F814W	$19.59^{+0.04}_{-0.00}$	$14.77^{+0.00}_{-0.21}$	$1.01^{+0.96}_{-0.01}$ / $3.63^{+0.96}_{-0.01}$	$3.6^{\vee}_{-0.8}$	$0.02^{\vee}_{-0.04}$	$10.77^{+70.42}_{\wedge}$ / $38.86^{+70.42}_{\wedge}$	$3.9^{+1.3}_{-0.0}$	$0.17^{+0.00}_{\wedge}$	$0.3^{+0.1}_{-0.0}$
SDSS-H5	F775W	$18.04^{+0.06}_{-0.01}$	$16.32^{+0.05}_{-0.22}$	$0.13^{+0.60}_{-0.08}$ / $0.55^{+0.60}_{-0.08}$	$1.2^{+0.7}_{-0.2}$	$0.07^{+0.32}_{-0.11}$	$4.65^{+57.66}_{-5.88}$ / $19.63^{+57.66}_{-5.88}$	$5.2^{+1.8}_{-0.5}$	$0.18^{+0.00}_{\wedge}$	$7.2^{+0.0}_{-0.0}$

$m^{\dagger}_{filter,corr}$ [mag]	$M^{\dagger}_{filter,0}$ [mag]	M/L [$M_\odot/L_\odot$]	$M_{\rm sph,*}$ [$M_\odot$]	M_{def} [$M_\odot$]	$\frac{M_{def}}{M_{\rm sph,*}}$ [%]	$\frac{M_{def}}{M_\bullet}$
(12)	(13)	(14)	(15)	(16)	(17)	(18)
$14.55^{+0.00}_{-0.21}$	$-25.69^{+0.00}_{-0.21}$	3.5	$4.44^{+0.96}_{\wedge} \times 10^{12}$	$1.75^{+1.31}_{-0.91} \times 10^{11}$	$3.9^{+1.80}_{-2.00}$	$6.9^{+30.3}_{+1.3}$
$16.03^{+0.05}_{-0.22}$	$-24.75^{+0.05}_{-0.22}$	3.5	$1.80^{+0.41}_{-0.09} \times 10^{12}$	$0.81^{+0.82}_{-0.40} \times 10^{11}$	$4.5^{+3.00}_{-2.00}$	$7.7^{+37.9}_{+1.6}$

Note. — Results of the core-Sérsic fit to the sample galaxies.
(1) Target name. (2) Reference filter for the magnitudes and surface brightnesses listed here. (3) Surface brightness at the core-Sérsic break radius. (4) Integrated apparent magnitude of the core-Sérsic model. (5) Break radius in units of arcseconds and kiloparsecs (the physical scale is provided in Table 1). (6) Alpha parameter for the core-Sérsic model. (7) Inner power-law index for the core-Sérsic model. (8) Effective radius (R_e) of the Sérsic portion of the core-Sérsic profile, in units of arcseconds and kiloparsecs. (9) Sérsic index. (10) Model ellipticity. (11) Model position angle (North = 0°). (12) Extinction and K-dimming corrected apparent magnitude. A galactic extinction of ∼0.07 mag (A2261-BCG) and 0.06 mag (SDSS-H5) was obtained from NED. We applied a K-correction of 0.15 mag (A2261-BCG) and 0.23 mag (SDSS-H5) following the prescriptions of Poggianti (1997) for early-type galaxies. In Poggianti (1997) and NED, we adopted the values for the Johnson-Cousins I and SDSS i bands as proxies for those of the HST $F814W$ and $F775W$ filters, respectively. (13) Absolute rest-frame magnitude of the object, adjusted for extinction and K-correction. Redshift dimming has been accounted for in the luminosity distances which we used to calculate the distance modulus (provided in Table 1). (14) Mass-to-light ratio (M/L; see §4 for details). (15) Model mass calculated assuming the M/L of column 14. (16) Mass deficit calculated from the luminosity deficit (L_{def}) assuming the M/L reported in column 14; L_{def} is in turn defined as the difference between the integrated luminosity of the extrapolation of the Sérsic part of the core-Sérsic model, and the luminosity of the core-Sérsic model itself. (17) Relative mass deficit. (18) Ratio of mass deficit to SMBH mass (from the $M_\bullet$ –$M_{\rm sph,*}$ relation, see Table 5). The errors reported in this table, which represent 50% confidence levels, reflect the uncertainty on the sky background (which dominates the error budget), and have been estimated using the Monte Carlo simulation presented in the Appendix. The ∨ and ∧ symbols represent upper and lower limits, respectively.
† Values refer to the AB mag system. The zero-point for the calibration is provided in the HST image header.

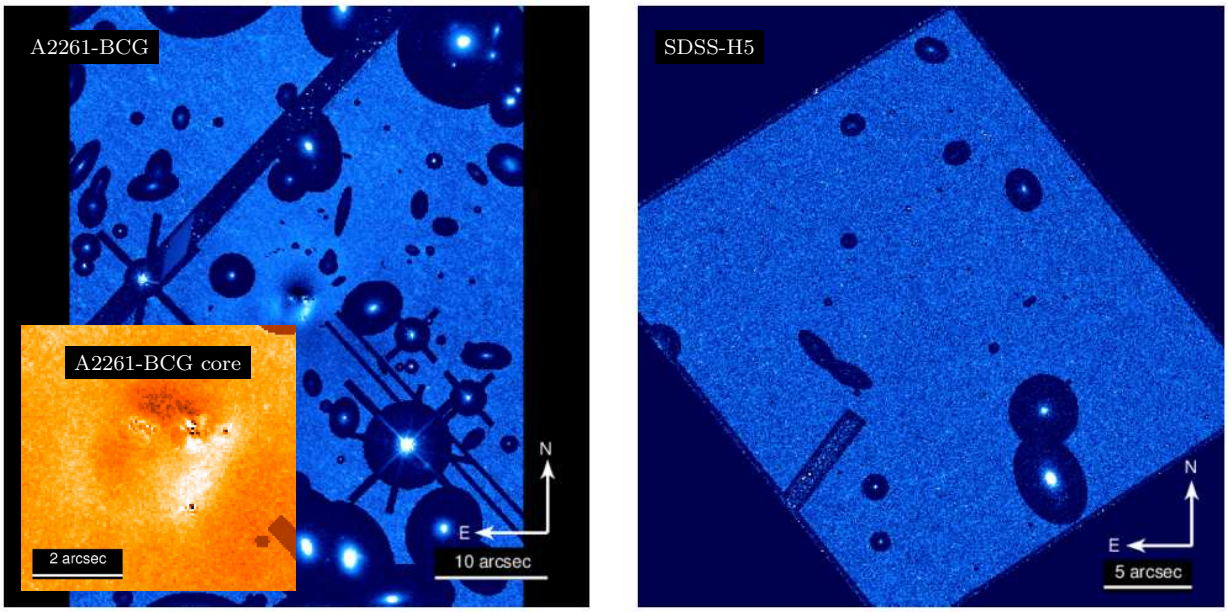

FIG. 2.— Residuals of the 2D fit to the image of A2261-BCG (*left*) and SDSS-H5 (*right*).
Residual images created by first subtracting the best-fit model produced by GALFIT-CORSAIR, and then normalizing by the "sigma" image. In this context, these images represent the residuals in units of standard deviation at each pixel position (and they are the equivalent of what we present in the bottom panels of Figure 3 for the 1D case). Masked objects have been down-scaled as in the top panels of Figure 1. Note: the left panel is a slightly zoomed area of that shown in the top-left panel of Figure 1. The insert in the left panel shows the separate fit performed on the innermost $5''$ square region of A2261-BCG to better constrain the models for the knots 1–5 (Table 3). The primary (dark / bright) dipole structure seen there is due to the isophote centroid shift, as a function of radius, seen in the lower-left panel of Figure 1. Note that the contrast used in the residual images has been maximised to better reveal the residual patterns. The 2D fit (data minus model) has $\Delta_\mu < 0.04$ mag arcsec^{-2} at all points, see also the 1D residual profile (Figure 3).

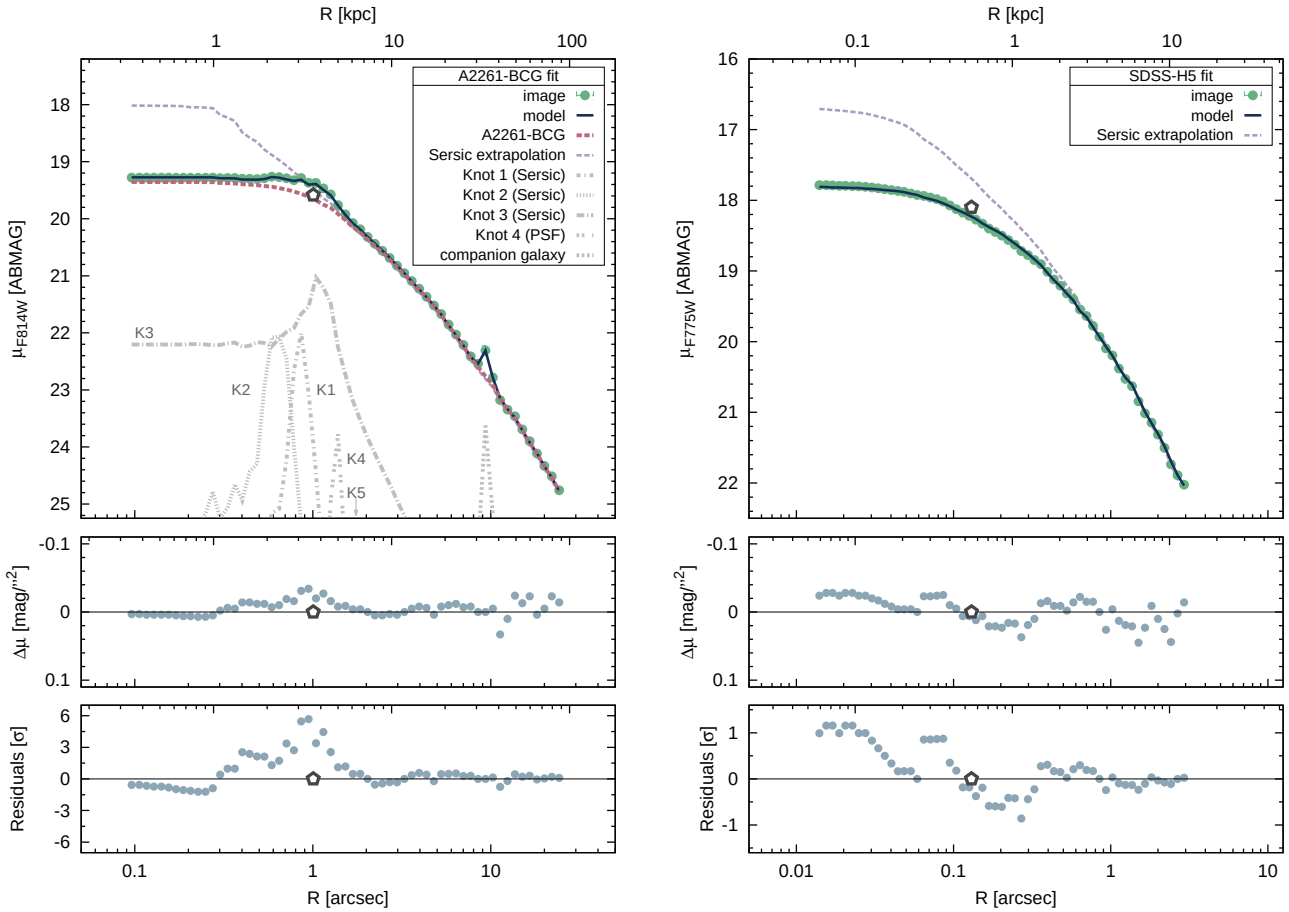

FIG. 3.— Projections of the results of the 2D fit to the image of A2261-BCG (*left*) and SDSS-H5 (*right*). The green data points represent the major-axis surface brightness profile measured over the isophotes defined using IRAF.*ellipse* (i.e. the same measurement presented in the bottom panel of Figure 1). The curves represent the surface brightness profile of the 2D model images measured over exactly the same isophotes. The continuous curves show the global [PSF-convolved] models, while the dashed curves below them represent their sub-components. The purple dashed lines show instead the projection of the 2D models created by extrapolating the Sérsic part of the core-Sérsic components. We stress that all these curves are *not* fits to the 1D profile, but rather surface brightness measurements (projections) of the 2D models, centered on the IRAF.*ellipse* centroids. This is also the reason for which the profiles of some components appear as offset, or present "wiggles". The projection of the surface brightness profiles of the knots 1–4 about the center of A2261-BCG are marked as K1–4 (the position of Knot 5 is indicated by an arrow). The pentagon indicates the location of the core-Sérsic model's break radius. Notice that this break radius is defined as the mid-point of the transition between the inner power-law and the outer Sérsic part of the core-Sérsic model (see the discussion in §3.2). The panels underneath the profiles represent the data residuals about the fitted models, first expressed in terms of the difference in surface brightness, and then in terms of residuals (in units of counts) divided by the standard deviation as measured on the "sigma" image. The projection for SDSS-H5 is limited by the largest isophote identified by IRAF.*ellipse*, and represents therefore only the inner $\sim 3''$ of the galaxy, while the actual 2D fit was extended to practically the whole image (see Figure 2).

centre. In terms of either a scoured mass or inhibited mass growth (which prevented completion of the Sérsic profile over the inner radii), this approach provides a central deficit which is equivalent to assuming that the original light profile was described by the outer Sérsic model over its entire radial extent.

As seen in Graham et al. (2003), intermediate-luminosity galaxies such as NGC 5831 have pure Sérsic light profiles over their entire radial extent, while fainter ETGs often display additional nuclear components relative to their Sérsic profile (e.g. Graham & Guzmán 2003). The luminosity deficit can then be converted into missing stellar mass assuming an M/L ratio. To do this, we first convert the absolute magnitudes into solar luminosities, using $M_{\odot,F814W} = 4.57$ mag[6] and $M_{\odot,F775W} = 4.53$ mag[7] for the absolute [AB] magnitude of the Sun. We report the M_{def} for our sample galaxies in Table 2, where we adopted the same M/L used to determine the galaxy total stellar mass (see also §3.2).

The percentage of stellar mass which is displaced from the core of a core-Sérsic galaxy is typically small ($\lesssim 1\%$) compared to the spheroid's total stellar mass, and it therefore usually does not affect the outer stellar distribution. In the case of A2261-BCG and SDSS-H5, the mass deficit accounts for a more significant fraction ($\gtrsim 4\%$; see Table 2) of the total mass of the spheroid. Therefore in this case there could be a small additional uncertainty in using the extrapolation of the Sérsic part of the core-Sérsic model as a proxy for the pre-depleted light profile. The mass deficit is high for SDSS-H5 due to

[6] www.ucolick.org/~cnaw/sun.html

[7] www.baryons.org/ezgal/filters.php

TABLE 3
Parameters for Knots 1–5 (A2261-BCG)

Object	Model	$m^{\dagger}_{F814W}$ [mag]	$m^{\dagger}_{F814W,corr}$ [mag]	$M^{\dagger}_{F814W,0}$ [mag]	M_* [$M_\odot$]
(1)	(2)	(3)	(4)	(5)	(6)
Knot 1	Sérsic	21.76	21.54	-18.70	7.09e+09
Knot 2	Sérsic	22.14	21.92	-18.32	5.00e+09
Knot 3	Sérsic	19.75	19.53	-20.71	4.52e+10
Knot 4	PSF	23.22	23.00	-17.24	1.86e+09
Knot 5	PSF	25.20	24.98	-15.26	2.98e+08

Note. — Results from simultaneously modelling the knots 1–5 and the inner 5″ (square).
(1) Target name. (2) Model. (3) Integrated apparent magnitude. (4) Extinction and K-corrected apparent magnitude. (see description in §3.2). (5) Absolute rest-frame magnitude of the object, adjusted for extinction and K-correction (distance modulus is provided in Table 1). (6) Stellar mass calculated assuming the same mass-to-light ratio used for A2261-BCG (3.5 $M_\odot/L_\odot$; see §4).
† Values refer to the AB mag system. The zero-point for the calibration is provided in the *HST* image header.

the broad transition region (i.e. low α) coupled with the large Sérsic index. The mass deficit relative to the predicted central SMBH mass is also given in Table 2. The predicted SMBH mass was obtained using the spheroid stellar mass and the scaling relation given by Scott et al. (2013) for early-type galaxies.

5. DISCUSSION

After excluding Holm 15A (Bonfini et al. 2015), the next two largest depleted cores reported in the literature were — to our knowledge — those of A2261-BCG (Postman et al. 2012), and SDSS-H5 (Hyde et al. 2008).

5.1. *Comparing our fit results with the literature*

Postman et al. (2012) fit the 1D light profile of A2261-BCG using a Nuker model (Lauer et al. 1995), while Hyde et al. (2008) used, in their analysis of SDSS-H5, both a Nuker and a core-Sérsic model. Rather than using the Nuker model "break radius" ($R_{b,Nuk}$) to designate the size of a depleted core, it is now common to adopt a "cusp radius" $R_{\gamma\prime=0.5}$, defined as the radius at which the negative logarithmic slope of the intensity profile ($\gamma\prime$) equals 0.5 (Carollo et al. 1997). For simplicity, hereafter we will denote $R_{\gamma\prime=0.5}$ as $R_{\gamma\prime}$. The parameter $R_{\gamma\prime}$ has been found to correlate better then $R_{b,Nuk}$ does with the galaxy properties (e.g. luminosity and stellar velocity dispersion; see Lauer et al. 2007). Moreover, when there is an actual break in the profile and a partially depleted core relative to the inward extrapolation of the outer Sérsic profile, $R_{\gamma\prime} = R_{b,cS}$ (Dullo & Graham 2013).

TABLE 4
Core Sizes

Target	$R_{\gamma\prime=0.5}$ (literature) [kpc]	$R_{b,cS}$ (literature) [kpc]	$R_{b,cS}$ (this work) [kpc]
(1)	(2)	(3)	(4)
A2261-BCG	3.2	-	3.63
SDSS-H5	0.6	1.5	0.55

Note. — Core sizes reported in the literature for A2261-BCG (Postman et al. 2012) and SDSS-H5 (Hyde et al. 2008).
(1) Target name. (2) Literature cusp radius (Nuker model). (3) Literature core-Sérsic break radius. (4) core-Sérsic break radius from Table 2.

Postman et al. (2012) report a projected cusp radius[8] $R_{\gamma\prime}$ of 3.2 kpc for A2261-BCG. From their Nuker fit of SDSS-H5, Hyde et al. (2008) reported $R_{b,Nuk}$ = 1.574 kpc and $R_{\gamma\prime} \sim 0.6$ kpc, while their core-Sérsic fit yielded a much larger break radius $R_{b,cS} = 1.541$ kpc, at odds with the observation that $R_{\gamma\prime}$ usually equals $R_{b,cS}$ (Dullo & Graham 2014). According to these core sizes (Table 4), A2261-BCG and SDSS-H5 currently represent the biggest core galaxies ever identified using a Nuker and a core-Sérsic model, respectively. For a comparison, the largest cusp radii of the other known Nuker core galaxies barely exceed ∼1 kpc (see Postman et al. 2012, their Figure 7), while the typical core-Sérsic galaxy usually hosts a core with $R_{b,cS}$ of a few hundred parsecs (e.g. Trujillo et al. 2004; Ferrarese et al. 2006; Richings et al. 2011; Dullo & Graham 2012, 2013, 2014; Rusli et al. 2013).

Our core-Sérsic fit to A2261-BCG confirmed that the galaxy has a large depleted core, rather than just a shallow inner light profile. The luminosity deficit (L_{def}) that we derived as the difference between the core-Sérsic profile and the inward extrapolation of its Sérsic part (see §4.1) is $\sim 1.43\times10^{11}$ $L_\odot$. This value is significantly higher than the luminosity deficit obtained by Postman et al. (2012) when subtracting their Nuker profile from the inward extrapolation of a Sérsic model fit to their marked-by-eye "envelope" of A2261-BCG ($M_{V,def}$ = −20.8 mag, or $L_{def} = 1.8\times10^{10}$ $L_\odot$).

The comparison with the results of Hyde et al. (2008) for SDSS-H5 requires some remarks. The large discrepancy between their core-Sérsic model's $R_{b,cS}$ and their Nuker model's $R_{\gamma\prime}$ (see Table 4), and between the R_e values they obtained from their core-Sérsic model and their Sérsic model fit of the galaxy (210.988 kpc and 13.907 kpc, respectively), raised our suspicion because when there *is* a depleted core, the (Nuker model)-derived value of $R_{\gamma\prime}$ and the core-Sérsic model's $R_{b,cS}$ are usually comparable (within a factor of 2; e.g. Dullo & Graham 2014), plus the core-Sérsic model's effective half-light ra-

[8] Throughout the paper, projected radii are expressed with a capital letter R.

dius is basically equal to the effective half light radius of the extrapolation of its Sérsic part (e.g. Trujillo et al. 2004). Moreover, the radial extent of their fit was limited to $\sim 7''$ (or $\sim$30 kpc; their Figure A3), corresponding to only $\sim$15% of the effective radius that they reported with the core-Sérsic model (211 kpc). This is in part what motivated us to perform our new core-Sérsic fit, which improved on the core-Sérsic fit by Hyde et al. (2008) in several aspects.

First, Hyde et al. (2008) adopted a simplified version of the core-Sérsic model, which assumed a sharp transition (i.e. $\alpha >> 1$; their Equation 2), while with GALFIT-CORSAIR we were able to fit an arbitrarily smooth transition. Given that we recover $\alpha \sim 1.2$, the assumption of a sharp transition is not appropriate for this galaxy, and led Hyde et al. (2008) to an excessively large $R_{b,cS}$. Notice that, from the physical point of view, low-alpha core-Sérsic galaxies are compatible with core excavation scenarios in the following terms. The scouring action, whether due to an in-falling perturber (see §5.3.2) or to a binary SMBH pair (see §5.3.1), need not occur only within the "break radius". The actual "loss cone" is more complicated than this, and works in the (position,velocity) phase space. Stars with large outer radii that plunge into the core of a galaxy can also be cleared/scoured away, and this would broaden the transition radius, and thus a low value of alpha need not indicate that the original profile was not described by a Sérsic model.

Second, we extended the radial fit range to $\sim 18''$ (or $\sim$75 kpc, which corresponds to $\sim$6 times our core-Sérsic R_e). Hyde et al. (2008) fit the surface brightness profile extracted along the major axis of the galaxy using a PSF-deconvolved image. The degeneracy related to the deconvolution process forced them to conservatively exclude the innermost $0.''035$ data, while with our 2D approach we could virtually fit the galaxy light up to the pixel scale limit ($0.''025$; see Table 1). Finally, Hyde et al. (2008) decided to apply equal weighting to each logarithmically-spaced data point to allow the inner data points to influence their fit more. In our 2D fit, we were able to weight the pixel independently, following the intrinsic Poissonian scatter (see §2.2). With this procedure we obtain a core-Sérsic break radius $R_{b,cS}$ = 0.6 kpc, significantly smaller than that of Hyde et al. (2008) (1.5 kpc), and in close agreement with their Nuker cusp radius $R_{\gamma'} = 0.6$ kpc.

5.2. *Predicting the cores size*

To put our galaxies in context with respect to the population of core-Sérsic objects, we can use the $R_{b,cS}$–luminosity relation for the spheroidal components of core-Sérsic galaxies to predict the core size expected for a spheroid with a given luminosity. We adopted the relation by Dullo & Graham (2014, their Table 3):

$$\log(R_{b,cS}\ pc) = (-0.45 \pm 0.05)(M_V + 22.0) + \\ +(1.79 \pm 0.06) \quad (3)$$

where M_V is the absolute luminosity in the V band. For A2261-BCG, we converted our absolute, rest frame magnitude $M_{F814W,0}$ to the V-band magnitude ($M_{V,0}^{\text{A2261-BCG}}$, Vega system) using the calibrations of Postman et al. (2012, their Equation 1 and Table 1), obtaining $M_{V,0}^{\text{A2261-BCG}} = -24.84$ mag. For SDSS-H5, we estimated the rest frame V-band magnitude ($M_{V,0}^{\text{SDSS-H5}}$, Vega system) by first converting our absolute, rest frame magnitude $M_{F775W,0}$ to the $F606W$ filter using the calibrations of Sirianni et al. (2005, their Table 29), and then using the $F606W$–V color conversions of Fukugita et al. (1995, their Table 3), obtaining $M_{V,0}^{\text{SDSS-H5}} = -23.66$ mag.

Using these magnitudes in Equation 3, we calculated an expected core radius of $\log(R_{b,cS}\ [\text{pc}]) = 3.07\ ^{+0.34}_{-0.35}$ ($1.2^{+0.9}_{-0.9}$ kpc) and $\log(R_{b,cS}\ [\text{pc}]) = 2.54\ ^{+0.32}_{-0.33}$ ($0.3^{+0.3}_{-0.3}$ kpc), for A2261-BCG and SDSS-H5 respectively[9]. Therefore, while the core of SDSS-H5 ($R_{b,cS}$ = 0.55 kpc) is compatible (within 1-σ) with what would be expected given its spheroid luminosity, the core of A2261-BCG ($R_{b,cS} = 3.63$ kpc) appears somewhat larger.

5.3. *Formation scenarios for the core*

We observe that, for both galaxies, the mass deficits account for $\gtrsim$4% of the stellar mass of their spheroids (see Table 2), almost one order of magnitude more than that found for the median depleted core (e.g Rusli et al. 2013; Dullo & Graham 2014). While our results relocate SDSS-H5 into the population of core-Sérsic objects with "standard-sized" cores ($\lesssim$ 1 kpc), they confirm the extraordinary large nature of the core in A2261-BCG. In this Section, we will explore two plausible formation scenarios for the creation of such an unusual core.

5.3.1. *The SMBH scouring scenario*

Several studies have highlighted a connection between the stellar mass (or light) deficit and the mass of the central black hole $M_\bullet$, which suggests the existence of an underlying link between the formation of the core and the central SMBH (e.g. Begelman et al. 1980; Faber et al. 1997; Ravindranath et al. 2002; Graham 2004; Ferrarese et al. 2006; Lauer et al. 2007; Kormendy & Bender 2009; Dullo & Graham 2014). These observational results have been supported by numerical simulations in the context of the scouring SMBH binary scenario (e.g. Milosavljević & Merritt 2001; Merritt 2006). In particular, the $M_\bullet$–M_{def} connection draws a quasi-linear relation in the log space, although with a large scatter. Here we test whether A2261-BCG follows this trend.

We predicted the expected, central black hole mass in A2261-BCG (and SDSS-H5) using our measured spheroid (*i*) stellar mass ($M_{\text{sph},*}$) and (*ii*) core break radius ($R_{b,cS}$).

(i) We adopt the 'core-Sérsic' $M_\bullet$–$M_{\text{sph},*}$ relation from Scott et al. (2013):

$$\log(M_\bullet/M_\odot) = (9.27 \pm 0.09) + \\ +(0.97 \pm 0.14) \log\left[M_{\text{sph},*}/3 \times 10^{11} M_\odot\right].$$

[9] The uncertainty calculated from Equation 3 was summed in quadrature with the intrinsic $\log(R_{b,cS})$ scatter of the data from which the equation was derived (0.3 dex; see Dullo & Graham 2014, their Table 1). Section 3.3 in Graham & Scott (2013) shows how this uncertainty is accounted for in the total error budget. The upper/lower errors on M_V (as well as on M_{sph} and R_b, used in §5.3) were estimated using the simulation presented in the Appendix, and are reported in Table 2).

TABLE 5
Predicted SMBH masses.

Galaxy	Parameter:value	$M_\bullet$ prediction $10^9\ M_\odot$
(1)	(2)	(3)
A2261-BCG	$M_{\rm sph,*}$: $4.44\times10^{12} M_\odot$	$25.4^{+21.4}_{-20.7}$
A2261-BCG	r_b: 3.63 kpc	$38.5^{+30.1}_{-28.6}$
SDSS-H5	$M_{\rm sph,*}$: $1.80\times10^{12} M_\odot$	$10.6^{+8.4}_{-8.1}$
SDSS-H5	r_b: 0.55 kpc	$6.8^{+8.5}_{-5.1}$

Note. — Black hole masses estimated using the scaling relations between $M_\bullet$ and the spheroid's stellar mass ($M_{\rm sph,*}$ Scott et al. 2013) and core break radius (R_b Rusli et al. 2013).
(1) Target name. (2) Parameter used for calculation. (3) Predicted SMBH mass.

where we used the spheroid masses reported in Table 2, i.e. 4.44×10^{12} $M_\odot$ and 1.80×10^{12} $M_\odot$ for A2261-BCG and SDSS-H5 respectively, and we assumed an intrinsic scatter of 0.3 dex in the $\log(M_\bullet)$ direction. The predicted black hole masses are provided in Table 5.

(ii) The $M_\bullet$–R_b relation from Rusli et al. (2013, their Equation 13: see also equations 15–17 in Dullo & Graham 2014) is such that:

$$\log(M_\bullet/M_\odot) = (10.07\pm0.16) + \\ +(0.92\pm0.20)\log\left[R_b[\mathrm{kpc}]\right],$$

and is reported to have an intrinsic scatter of 0.28 dex in the $\log(M_\bullet)$ direction. Assuming a 20% uncertainty on our break radii, the predicted black hole masses are given in Table 5. We note that the SMBH mass predicted here for A2261-BCG will be too high if its unusually large core was not formed via the same mechanism that formed the cores in the spheroids that were used to construct the $M_\bullet$–R_b relation.

In addition to these estimates, for A2261-BCG we can consider $M_\bullet$ from the relation of Merloni et al. (2003) between the SMBH activity (in radio and X-ray bands) and the SMBH mass (also considered in Postman et al. 2012). This yields $M_\bullet \sim 2.0\times10^{10}$ $M_\odot$ (Hlavacek-Larrondo et al. 2012). Notice that all of the $M_\bullet$ reported here for A2261-BCG are comparable to, or supersede the largest black hole mass dynamically measured (NGC 4889; $M_\bullet = 2.1\times10^{10}$ $M_\odot$; McConnell et al. 2011).

We can now estimate the $M_{def}/M_\bullet$ ratio (see Table 2) and compare this figure with the predictions of the numerical simulations by Merritt (2006) for the SMBH scouring scenario. Merritt (2006) suggested that M_{def} $\propto 0.5NM_\bullet$, where N is the effective number of major dry (i.e. gas poor) mergers which the galaxy experienced. This picture would imply that A2261-BCG (and SDSS-H5) underwent some 14 consecutive dry major mergers (*and* no wet merger able to refill the core), which is more than expected from any evolutionary scenario of galaxies. Moreover, the semi-analytical simulations of De Lucia & Blaizot (2007) suggest that most of the stellar mass of a BCG is assembled through *minor* mergers at high redshifts, and with very few major dry mergers.

Black holes can be responsible for the ejection of stars even beyond the binary SMBH phase, after its coalescence, such as in the "ejected SMBH" scenario in which anisotropic emission of gravitational radiation results in the SMBH being shot off in the opposite direction. An interesting corollary to this scenario is that the displaced SMBH might carry along a "cloak" of stars (Merritt et al. 2009). Postman et al. (2012) investigated this hypothesis for A2261-BCG, and suggested that knot 4 (see Figure 1) represents the most suitable candidate for a stellar cloak around an ejected SMBH. The projected isophotes of partially-depleted cores have been measured to be rather round (Dullo & Graham 2015), and as such they are not suggestive of highly eccentric orbits. The lack of such orbits is expected to delay the merger event since the SMBH binary takes longer to reach the close separation regime, when gravitational radiation becomes strong enough to lead the binary to a rapid coalescence (Thorne 1992; Haehnelt 1994; Jaffe & Backer 2003; Sesana 2013). The upshot is that there may be more mergers later on, i.e. more recently, whose gravitational radiation we can detect today.

5.3.2. *The stalled perturber scenario*

We evaluate the "stalled perturber" scenario (e.g. Goerdt et al. 2010) in which the baryonic core of A2261-BCG has been excavated by a massive, compact object which fell into the galaxy. Clearly, in this case, knots 1–5 represent obvious candidate perturbers. We will base our investigation on the following predictions from numerical simulations.

It has been shown that once a flat density core is created, dynamical friction no longer applies and the in-spiralling object will "stall" at the boundary of the core (Goerdt et al. 2006; Read et al. 2006a; Inoue 2009, 2011). The insert in the left panel of Figure 1 represents with a dashed region the extent of the core of A2261-BCG, as we measured with our core-Sérsic fit, and centered in the center of our Galfit-Corsair model fit to the inner $5''$ region. From the image we can only infer the de-projected position of the knots with respect to the core center. Therefore every object within and on the circle, nominally knots 1–3, is a possible perturber.

It is expected that the core radius should roughly correspond to the radius within which the enclosed (pre-depletion) mass equals the mass of the perturber (Read et al. 2006b; Goerdt et al. 2010). We can approximate the original mass enclosed within $R_{b,cS}$ (M_{enc}) as:

$$M_{enc} \sim M_{core} + M_{def,core} \quad (4)$$

where M_{core} is the stellar mass still observed within the depleted core, and $M_{def,core}$ is the mass deficit calculated only within $R_{b,cS}$. We calculated M_{core} from the deprojected luminosity density profile reported in Postman et al. (2012, their Figure 6), which has been obtained from an Abel inversion of their Nuker surface brightness profile.[10] According to their results,

[10] In particular, we consider the simplest model of Postman et al. (2012), where the inner slope γ of the Nuker model was held fixed at a value of 0.

the central luminosity density ($\rho_{L,c}$) is roughly constant ($\sim$0.03 $L_\odot$ pc^{-3}) up to the core radius. The stellar mass still enclosed by the core is thus:

$$M_{core} = \frac{4}{3}\pi(R_{b,cS})^3\ \rho_{L,c}\ (M/L) \quad (5)$$

where $R_{b,cS}$ is our best-fit core-Sérsic core radius, and M/L is the same mass-to-light ratio assumed to calculate the galaxy mass (see §4). We note that this approximation smooths over the caveat that the Nuker model overestimates the outer profile of the galaxy, hence it underestimates the resulting central density. In this way, we calculated $M_{core} = 2.1\times10^{10}\ M_\odot$. $M_{def,core}$ is $11.7\times10^{10}\ M_\odot$; this value is smaller than the M_{def} reported in Table 2 ($17.5\times10^{10}\ M_\odot$) due to our use of the mass deficit within the spherical volume bounded by $R_{b,cS}$ and the smooth transition between the power-law and the Sérsic domains of the core-Sérsic model (formally, the Sérsic extrapolation "detaches" from the core-Sérsic profile at infinite radii). Ultimately, these quantities yielded $M_{enc} = 13.8\times10^{10}\ M_\odot$.

We compare this value against the mass of knot 3, the most luminous object around the core of A2261-BCG. Its mass ($M_{knot\ 3} = 4.5\times10^{10}\ M_\odot$; see Table 3) is a factor of $\sim$3 smaller than M_{enc}. However, the actual mass comparison should be performed against the mass of the infalling perturber *before* the dynamical interaction, during which the perturber itself could have lost stellar mass. Moreover, the extended wings of knot 3 might be confused with the underlying light of the galaxy; this may have reduced the object luminosity recovered by our fit. Given these considerations, knot 3 represents a plausible candidate perturber to explain the unusually large radial extent of the core in A2261-BCG. Knots 1 and 2 might have contributed to the excavation of the core (although to a lesser extent) through an analogous infall process.

Finally, if the core has been excavated by an object spiralling into the galaxy center, shredding the central cuspy distribution and producing asymmetrical features (e.g., see Figure 5 in Goerdt et al. 2010), then the brightness centroid is expected to shift inside the core radius, as we in fact observe (shift $\sim 0''.05 - 0''.1$; see §3.2). However, a centroid displacement would be expected as well in the "ejected SMBH" scenario explored by Postman et al. (2012).

Both our results and those of Postman et al. (2012) rule out the simple binary SMBH scenario for the formation of the core of A2261-BCG, unless the binary has already coalesced and the core has been formed/enlarged by the ejection of the SMBH. As already pointed out by Postman et al. (2012), a core lacking its central SMBH would be "exposed" to refilling from dense in-falling satellites, implying that — in this scenario — the core of A2261-BCG is particularly young.

6. CONCLUSIONS

We have investigated two galaxies reported to have the largest depleted cores according to a Nuker and a core-Sérsic fit, namely the BCG of Abell 2261 (A2261-BCG; $R_{\gamma\prime} = 3.2$ kpc; Postman et al. 2012) and SDSS-J091944.2+562201.1 (SDSS-H5; $R_{b,cS} = 1.54$ kpc; Hyde et al. 2008), respectively. We have modelled the two-dimensional surface brightness distribution of the galaxies with a 2D core-Sérsic model, using GALFIT-CORSAIR (Bonfini 2014).

From our fit, we obtained a core-Sérsic break radius $R_{b,cS} \sim 0.55$ kpc for SDSS-H5, a value 3 times smaller than the $R_{b,cS}$ reported by Hyde et al. (2008), and compatible with their cusp radius $R_{\gamma\prime} = 0.6$ kpc. We attribute this large discrepancy to the fact that Hyde et al. (2008) used a simplified formulation of the core-Sérsic model, assuming a sharp transition between the Sérsic and the power-law, while our fit revealed that the transition is instead very smooth ($\alpha \sim 1.2$; §5.1). This led Hyde et al. (2008) to derive an exceptionally large $R_{b,cS}$. Given this result, we note that it would be worth re-investigating the other galaxies in Hyde et al. (2008), in particular those reported to have large cores.

We performed a core-Sérsic fit to A2261-BCG, and found $R_{b,cS} = 3.6$ kpc (§4), confirming the existence of the unusually large depleted core first claimed by Postman et al. (2012) using the cusp radius. With this $R_{b,cS}$, A2261-BCG can now be reported to have the biggest core of any core-Sérsic galaxy. The core radius of A2261-BCG is three times the value expected from the $R_{b,cS}$–M_V relation of Dullo & Graham (2014) for core-Sérsic galaxies (§5). We have calculated the stellar mass deficit associated with the core of A2261-BCG from the extrapolation its outer profile, obtaining $M_{def} \sim 1.75\times10^{11}\ M_\odot$ (§4.1).

Moreover, we compared M_{def} against the expected mass of the central black hole ($M_\bullet$), which we estimated using the spheroid stellar mass (§5.3.1, Table 5). The predicted black hole mass ($25 \times 10^9\ M_\odot$) exceeds the most massive SMBH mass that has ever been directly measured, and yields $M_{def}/M_\bullet \approx 7$. This result is in disagreement with the simple (i.e. no gravitational-wave recoil) SMBH binary scouring scenario given the unrealistic number of major mergers it would imply, unless the core was subsequently enlarged by the rebound following the ejection of the coalesced binary (§5.3.1). Given this high $M_{def}/M_\bullet$ ratio *and* the unusually large core radius, we therefore explored the "stalled perturber" model (e.g. Goerdt et al. 2006; Read et al. 2006a,b; Inoue 2009; Goerdt et al. 2010; Inoue 2011). According to this scheme, a captured object spiralling inward excavated the core of A2261-BCG via dynamical friction, and finally settled at the $R_{b,cS}$ radial distance from the galaxy center once the friction process lost efficiency. There are several objects about the core of A2216-BCG, three of which fall — along the line of sight — within the core ("knots 1–3"; Figure §1). By testing the prediction that the mass within the core should match the mass of the perturber (e.g. Read et al. 2006b; Goerdt et al. 2010), we suggest that knot 3 (or a combination of the scouring actions of knots 1–3) might be responsible for the creation of the core of A2261-BCG.

Discerning the definitive truth about A2261-BCG could benefit from a direct (dynamical) detection, location, and measurement of the mass of its black hole, and accurate spectroscopy of the knots about the core in order to determine their relative velocity and age. In any case, our results on A2261-BCG (together with those of Postman et al. 2012) pose a critical challenge to the simple binary SMBH scenario as the only mechanism of core-formation, and calls for additional, careful studies of

high-mass core-Sérsic galaxies. The "stalled perturber" model proved to be plausible for the explanation of the large depleted core in A2261-BCG, and is worth consideration in future investigations.

The authors wish to thank Tobias Goerdt for providing useful clarifications regarding the "stalled perturber" scenario. We are also very grateful to David Merritt for reviewing parts of this paper. Finally, we thank T. Bitsakis and A. Zezas for their assistance during the review process. This research was supported under the Australian Research Councils funding scheme (FT110100263). This research has made use of the NASA/IPAC Extragalactic Database (NED). Based on observations made with the NASA/ESA Hubble Space Telescope, obtained from the data archive at the Space Telescope Science Institute. STScI is operated by the Association of Universities for Research in Astronomy, Inc. under NASA contract NAS 5-26555. The HST observations are associated with GO proposal 12066 (PI: Postman, M.), and SNAP proposal 10199 (PI: Bernardi, M.).

REFERENCES

Abazajian, K., Adelman-McCarthy, J. K., Agüeros, M. A., et al. 2003, AJ, 126, 2081
Begelman, M. C., Blandford, R. D., & Rees, M. J. 1980, Nature, 287, 307
Bertin, E., & Arnouts, S. 1996, A&AS, 117, 393
Bekenstein, J. D. 1973, ApJ, 183, 657
Bonfini, P. 2014, PASP, 126, 935
Bonfini, P., Dullo, B. T., & Graham, A. W. 2015, arXiv:1506.08560
Boylan-Kolchin, M., Ma, C.-P., & Quataert, E. 2004, ApJ, 613, L37
Carollo, C. M., Franx, M., Illingworth, G. D., & Forbes, D. A. 1997, ApJ, 481, 710
Chandrasekhar, S. 1943, ApJ, 97, 255
Ciambur, B. C. 2015, ApJ, 810, 120
De Lucia, G., & Blaizot, J. 2007, MNRAS, 375, 2
Donzelli, C. J., Muriel, H., & Madrid, J. P. 2011, ApJS, 195, 15
Dressel, L., 2015. "Wide Field Camera 3 Instrument Handbook, Version 7.0" (Baltimore: STScI)
Dullo, B. T., & Graham, A. W. 2012, ApJ, 755, 163
Dullo, B. T., & Graham, A. W. 2013, ApJ, 768, 36
Dullo, B. T., & Graham, A. W. 2014, MNRAS, 444, 2700
Dullo, B. T., & Graham, A. W. 2015, ApJ, 798, 55
Ebisuzaki, T., Makino, J., & Okumura, S. K. 1991, Nature, 354, 212
El-Zant, A., Shlosman, I., & Hoffman, Y. 2001, ApJ, 560, 636
El-Zant, A. A., Hoffman, Y., Primack, J., Combes, F., & Shlosman, I. 2004, ApJ, 607, L75
Emsellem, E. 2013, MNRAS, 433, 1862
Faber, S. M., Tremaine, S., Ajhar, E. A., et al. 1997, AJ, 114, 1771
Ferrarese, L., Côté, P., Jordán, A., et al. 2006, ApJS, 164, 334
Fitchett, M. J., & Detweiler, S. 1984, MNRAS, 211, 933
Freedman D., Diaconis P. 1981, Probability Theory and Related Fields, Springer, Berlin
Fruchter, A. S. , Hack, W., Dencheva, N., Droettboom, M., et al., 2010, "BetaDrizzle: A Redesign of the MultiDrizzle Package" in STSCI Calibration Workshop Proceedings, Baltimore, MD, 21-23 July 2010, eds. Susana Deustua & Cristina Oliveira, Space Telescope Science Institute, pp 376 - 381
Fukugita, M., Shimasaku, K., & Ichikawa, T. 1995, PASP, 107, 945
Gallazzi, A., Charlot, S., Brinchmann, J., & White, S. D. M. 2006, MNRAS, 370, 1106
Goerdt, T., Moore, B., Read, J. I., Stadel, J., & Zemp, M. 2006, MNRAS, 368, 1073
Goerdt, T., Moore, B., Read, J. I., & Stadel, J. 2010, ApJ, 725, 1707
González, J. A., Hannam, M., Sperhake, U., Brügmann, B., & Husa, S. 2007, Physical Review Letters, 98, 231101
Graham, A. W. 2004, ApJ, 613, L33
Graham, A. W., Erwin, P., Trujillo, I., & Asensio Ramos, A. 2003, AJ, 125, 2951
Graham, A. W., & Guzmán, R. 2003, AJ, 125, 2936
Graham, A. W., & Scott, N. 2013, ApJ, 764, 151
Graham, A. W., Durré, M., Savorgnan, G. A. D., et al. 2016, ApJ, 819, 43
Gualandris, A., & Merritt, D. 2008, ApJ, 678, 780
Haehnelt, M. G. 1994, MNRAS, 269, 199
Hlavacek-Larrondo, J., Fabian, A. C., Edge, A. C., & Hogan, M. T. 2012, MNRAS, 424, 224
Holley-Bockelmann, K., & Khan, F. M. 2015, arXiv:1505.06203
Huang, S., Ho, L. C., Peng, C. Y., Li, Z.-Y., & Barth, A. J. 2013, ApJ, 766, 47
Hyde, J. B., Bernardi, M., Sheth, R. K., & Nichol, R. C. 2008, MNRAS, 391, 1559
Khan, F. M., Holley-Bockelmann, K., Berczik, P., & Just, A. 2013, ApJ, 773, 100
King, I. R., & Minkowski, R. 1966, ApJ, 143, 1002
King, I. R., & Minkowski, R. 1972, External Galaxies and Quasi-Stellar Objects, Proceedings from IAU Symposium no. 44 held in Uppsala, Sweden, 10-14 August 1970. Edited by David Stanley Evans, Derek Wills, and Beverly J. Wills. International Astronomical Union. Symposium no. 44, Dordrecht, Reidel, p.87
Kormendy, J. 2009, Galaxy Evolution: Emerging Insights and Future Challenges, 419, 87
Kormendy, J., & Bender, R. 2009, ApJ, 691, L142
Krist, J. E., Hook, R. N., & Stoehr, F. 2011, Proc. SPIE, 8127
Kulkarni G., Loeb A., 2012, MNRAS, 422, 1306
Jaffe, A. H., & Backer, D. C. 2003, ApJ, 583, 616
Jedrzejewski, R. I. 1987, MNRAS, 226, 747
Inoue, S. 2009, MNRAS, 397, 709
Inoue, S. 2011, MNRAS, 416, 1181
Laine, S., van der Marel, R. P., Lauer, T. R., et al. 2003, AJ, 125, 478
Lauer, T. R., Ajhar, E. A., Byun, Y.-I., et al. 1995, AJ, 110, 2622
Lauer, T. R., Faber, S. M., Richstone, D., et al. 2007, ApJ, 662, 808
López-Cruz, O., Añorve, C., Birkinshaw, M., et al. 2014, ApJ, 795, LL31
Madrid, J. P., & Donzelli, C. J. 2016, ApJ, 819, 50
Markakis, K., Dierkes, J., Eckart, A., et al. 2015, A&A, 580, A11
Martizzi, D., Teyssier, R., & Moore, B. 2012, MNRAS, 420, 2859
McConnell, N. J., Ma, C.-P., Gebhardt, K., et al. 2011, Nature, 480, 215
McNamara, B. R., Kazemzadeh, F., Rafferty, D. A., et al. 2009, ApJ, 698, 594
Merloni, A., Heinz, S., & di Matteo, T. 2003, MNRAS, 345, 1057
Merritt, D., & Milosavljević, M. 2002, Proceedings of the International Conference DARK, Cape Town, South Africa. H. V. Klapdor-Kleingrothaus, R. D. Viollier (eds.). Physics and astronomy online library. Berlin: Springer, ISBN 3-540-44257-X, 2002, p. 79 - 89
Merritt, D., Milosavljević, M., Favata, M., Hughes, S. A., & Holz, D. E. 2004, ApJ, 607, L9
Merritt, D., Piatek, S., Portegies Zwart, S., & Hemsendorf, M. 2004, ApJ, 608, L25
Merritt, D., & Milosavljević, M. 2005, Living Reviews in Relativity, 8, 8
Merritt, D. 2006, ApJ, 648, 976
Merritt, D., Schnittman, J. D., & Komossa, S. 2009, ApJ, 699, 1690
Merritt, D. 2015, ApJ, 804, 128
Milosavljević, M., & Merritt, D. 2001, ApJ, 563, 34
Milosavljević, M., & Merritt, D. 2003, The Astrophysics of Gravitational Wave Sources, AIP Conference Proceedings, Volume 686, pp. 201-210
Peng, C. Y., Ho, L. C., Impey, C. D., & Rix, H.-W. 2010, AJ, 139, 2097
Petts, J. A., Gualandris, A., & Read, J. I. 2015, MNRAS, 454, 3778
Pinkney, J., Gebhardt, K., Bender, R., et al. 2003, ApJ, 596, 903
Poggianti, B. M. 1997, A&AS, 122, 399
Postman, M., Lauer, T. R., Donahue, M., et al. 2012, ApJ, 756, 159
Quinlan, G. D. 1996, NewA, 1, 35
Ravindranath, S., Ho, L. C., & Filippenko, A. V. 2002, ApJ, 566, 801
Read, J. I., Goerdt, T., Moore, B., et al. 2006, MNRAS, 373, 1451
Read, J. I., Wilkinson, M. I., Evans, N. W., Gilmore, G., & Kleyna, J. T. 2006, MNRAS, 366, 429
Redmount, I. H., & Rees, M. J. 1989, Comments on Astrophysics, 14, 165
Richings, A. J., Uttley, P., Körding, E. 2011, MNRAS, 415, 2158
Rusli, S. P., Erwin, P., Saglia, R. P., et al. 2013, AJ, 146, 160

Scott, N., Graham, A. W., & Schombert, J. 2013, ApJ, 768, 76
Seigar, M. S., Graham, A. W., & Jerjen, H. 2007, MNRAS, 378, 1575
Sesana, A. 2013, Classical and Quantum Gravity, 30, 244009
Shankar, F., Calderone, G., Knigge, C., et al. 2016, arXiv:1601.02021
Sirianni, M., Jee, M. J., Benítez, N., et al. 2005, PASP, 117, 1049
Thorne, K.S. 1992, in Sources of gravitational waves and prospects for their detection, A.I. Janis, J.R. Porter (Eds.), Recent Advances in General Relativity, Birkhäuser (1992), pp. 196-229
Tonini, C., Lapi, A., & Salucci, P. 2006, ApJ, 649, 591
Trujillo, I., Graham, A. W., & Caon, N. 2001, MNRAS, 326, 869
Trujillo, I., Erwin, P., Asensio Ramos, A., & Graham, A. W. 2004, AJ, 127, 1917
Vaccari, M. 2000, Masters Thesis
van den Bosch, R. C. E., Gebhardt, K., Gültekin, K., et al. 2012, Nature, 491, 729
Vasiliev, E., Antonini, F., & Merritt, D. 2015, ApJ, 810, 49
Walsh, J. L., van den Bosch, R. C. E., Gebhardt, K., et al. 2015, ApJ, 808, 183
Worthey, G. 1994, ApJS, 95, 107
Yu, Q. 2002, MNRAS, 331, 935

APPENDIX

The sky background is arguably the main source of uncertainty in the 2D fit of galaxy surface brightnesses. In the cases in which the galaxy occupies a large fraction of the image frame, it is virtually impossible to recover the true value of the sky, as one cannot disentangle the contribution due to the "wings" of the galaxy light itself (unless of course the intrinsic galaxy light distribution was known a-priori).

One possible approach to overcome this limitation consists in investigating the sky values recovered from a pool of sky + galaxy fits performed at different frame coverages (i.e. relative frame sizes with respect to the galaxy size; e.g. Huang et al. 2013). We preferred instead to adopt an approach which is completely independent from the model assumed to describe the galaxy light, in order to measure the uncertainties on the best-fit parameters due to our lack of information about the sky.

We started from the consideration that — in the most conservative scenario — the true sky value of a galaxy-dominated image could be anything between the background value measured at the image borders (i.e. the whole background is due to the sky brightness), and 0 (i.e. the background is totally dominated by the galaxy light)[11]. To evaluate the possible range of the fit parameters, we therefore run 50 new fits using different fixed background values, uniformly sampled between the aforementioned limits. At each run, all the core-Sérsic parameters were left free to vary. We adopted the same sigma image as for our actual fit in order to be able to compare the resulting best-fit χ^2.

As expected, most of the fits run for background values very different from the assumed background failed (i.e. did not converge). For the valid fits, the distribution of each best-fit parameter was constructed by binning the data according to the Freedman-Diaconis prescription (Freedman & Diaconis 1981), after weighting each value by the χ^2 of the corresponding fit. The resulting distributions are presented in Figure 4. Notice that, by encompassing *all* the possible sky values, these histograms actually play the role of Probability Distribution Functions (PDFs). It is therefore possible to use them to calculate the Confidence Levels (CLs) around the actual best-fit parameters (indicated by the green arrows). The 50% CLs are shown in the figures with dashed lines (and reported in Table A.1).

We observe that — as expected — most of the parameters present a skewed PDF, indicating a monotonic trend of the parameter with respect to the background level. For this reason, most of the best-fit parameters turn out to be upper/lower limits. In particular, the Sérsic index and the effective radius appear to show the stronger dependence on the background[12]. The parameters which are obviously insensitive to the background level, such as the P.A. and axis ratio, vary stochastically among the simulated fits, and hence present flatter distributions with smaller relative widths.

Finally, in order to determine the uncertainties upon the integrated quantities (total magnitude, mass, mass deficit, and mass deficit to total mass ratio) we adopted a similar approach. Nominally, we calculated those quantities for each of the simulated fit, and then adopted the 50% CLs around each [best-fit] quantity as an estimate of its error. The probability distributions for the integrated quantities are shown in the Figure 5.

[11] Recall that the the sky value we adopted in our best-fit (which we will label "assumed background" and "actual fit", respectively) was measured at the image borders, and hence corresponds to the assumption that the whole background is due to the sky.

[12] Notice that on top of the background dependence, the Sérsic index and the effective radius of the Sérsic model also present a true covariance (e.g. Trujillo et al. 2001).

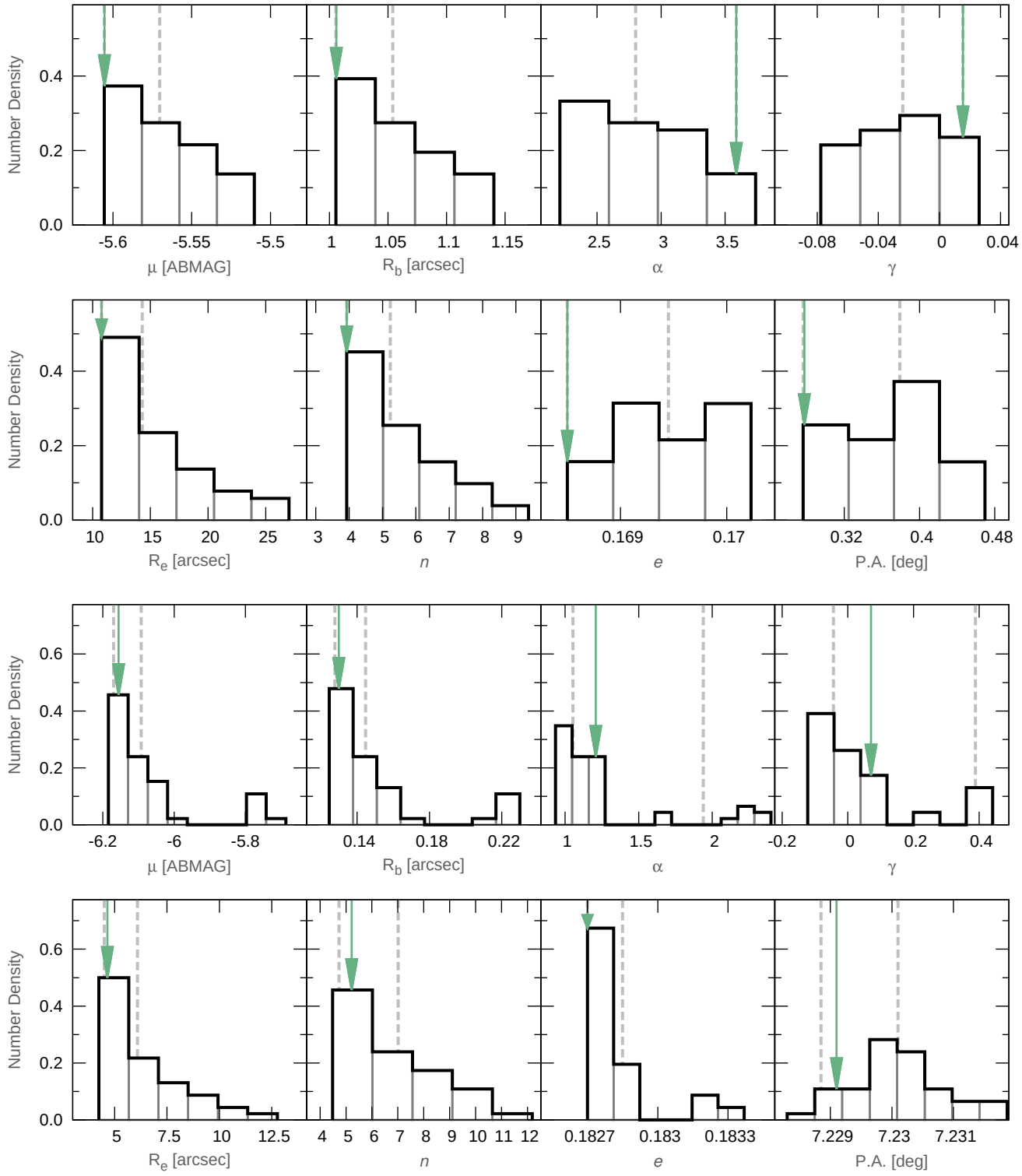

FIG. 4.— Confidence Levels (CLs) for the best-fit core-Sérsic parameters of A2261-BCG (*top*) and SDSS-H5 (*bottom*). The histograms show the probability distribution functions of the core-Sérsic parameters derived from fits performed adopting different background levels. The green arrows show the values of the actual best-fit parameters (i.e., the ones reported in Table 2), while the dashed lines represent the 50% CLs around them.
NOTE: The fact that best-fit values (and CLs) which are upper limits (e.g. α and γ for A2261-BCG) do not appear at the edge of the rightmost bin is just a representation side-effect due to the binning scheme, which starts from the leftmost data point, and increases with a fixed Freedman-Diaconis bin size.

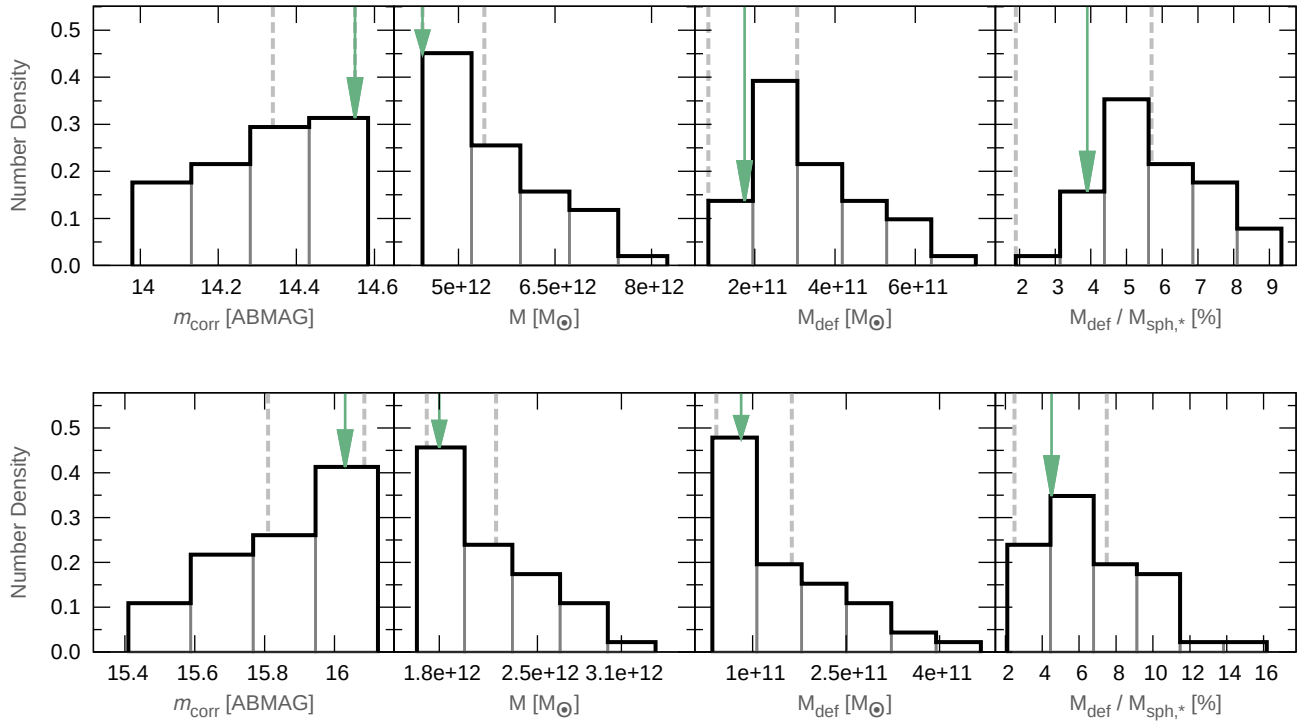

FIG. 5.— Confidence Levels (CLs) for the integrated core-Sérsic properties of A2261-BCG (*top*) and SDSS-H5 (*bottom*). The histograms represent the probability distribution functions for the (from left to right) extinction and K-dimming corrected apparent magnitude, spheroid stellar mass, mass deficit, and mass deficit to spheroid mass ratio, obtained simulating fits with different background levels. As for Figure 4, the green arrows show the values corresponding to our actual best-fit (Table 2), while the dashed lines represent the 50% CLs around them.